ACS APPLIED ENERGY MATERIALS

www.acsaem.org Article

Improved Electrochemical Properties of $Li_4Ti_5O_{12}$ Nanopowders (NPs) via Addition of $LiAlO_2$ and Li_6SiON Polymer Electrolytes, Derived from Agricultural Waste

Eleni Temeche,* Elizaveta Buch, Xinyu Zhang, Taylor Brandt, Andreas Hintennach, and Richard M. Laine*

Cite This: *ACS Appl. Energy Mater.* 2021, 4, 1894−1905 Read Online

ACCESS | Metrics & More | Article Recommendations | Supporting Information

ABSTRACT: $Li_4Ti_5O_{12}$ (LTO) has received considerable interest as an alternate anode material for high power density batteries for large scale applications. However, LTO suffers from poor Li^+ diffusivity and poor electronic conductivity, resulting in capacity loss and poor rate performance. Here we demonstrate a facile synthesis of LTO NPs using liquid-feed flame spray pyrolysis (LF-FSP) which provides high surface area (~38 m^2/g) spinel structure LTO NPs with average particle sizes (APSs) of 45 ± 0.3 nm. Pristine LTO-Li half-cells exhibit reversible capacity of 70 mAh/g at 10 C. In this study, we show that mixing $LiAlO_2$ NPs (5 wt %) and Li_6SiON polymer precursor (10 wt %) with pristine LTO via ball-milling and ultrasonication followed by tape casting enhances the LTO rate performance providing reversible capacity of ~217 mAh/g at 5 C over 500 cycles. The Li_6SiON polymer electrolyte is synthesized from rice hull ash (RHA), an agricultural waste, providing a green synthetic approach to electrode coating materials. CV and EIS studies indicate that adding the solid and polymer electrolytes reduces charge-transfer resistance and electrode polarization, enhancing both reversibility and the LTO Li^+ diffusion coefficient from 4.6×10^{-14} to 2.7×10^{-12} cm^2/s.

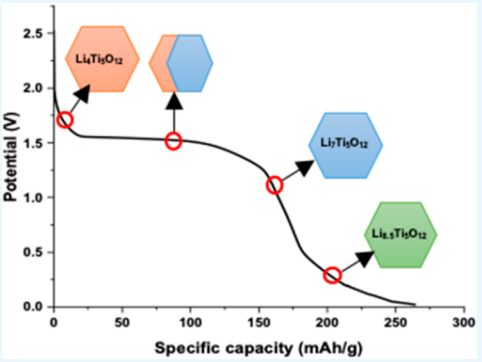

KEYWORDS: *$Li_4Ti_5O_{12}$, $LiAlO_2$, Li_6SiON, polymer precursor, nanopowders, anode, rate capability*

1. INTRODUCTION

Lithium-ion batteries (LIBs) are used extensively in electronics, electric vehicles, stationary power storage, and a multitude of related renewable energy applications attributed to their high energy and power densities.[1,2] However, in current designs, LIBs based on commercial carbonaceous anode materials cannot meet the fast charge capabilities required for many large-scale applications due to serious safety problems associated with high charge/discharge rates.[3,4]

Given the low galvanostatic potential (~0 vs Li^+/Li) of current graphitic anodes,[5,6] higher charging rates may cause (especially uneven) lithium plating generating internal short-circuits leading to catastrophic failure of traditional LIBs.[7,8] Thus, to enable fast charging and improve LIB safety; numerous noncarbonaceous anodes have been explored.[9−11] Among the possible alternate anode materials, LTO has been considered very promising due to its excellent thermal stability, high structural stability, good cyclability at high current densities, and negligible irreversible capacity.[12−14]

Spinel LTO anodes can facilitate up to three Li^+ ions per formula unit and deliver theoretical capacities ~175 mAh g^{-1} without significant volume changes (<1%) when cycled.[15−17] Graphite anodes in contrast expand up to 10 vol % during charging.[12] This negligible volume change (zero-strain) property of LTO provides high structural stability, potentially enabling high charge/discharge rates thereby improving LIBs' versatility.[12,18,19] In addition, LTO's operating potential is greater than the reduction voltage of conventional electrolyte solvents (propylene carbonate and ethylene carbonate), an attractive feature for rate performance.[20,21]

Unfortunately, pristine spinel LTO exhibits poor electronic conductivity (10^{-13} S cm^{-1})[22] attributed to the Ti^{4+} valence state and low Li^+ diffusion coefficient (10^{-9}−10^{-14} cm^2 s^{-1}) resulting in capacity loss and poor rate capability, which limits its usage in practical applications.[22−24] To date, numerous methods have been explored to ameliorate the electronic conductivity and Li^+ diffusivity.[12,25−27] The most common method focuses on doping with metallic (Cr^{3+}, Ca^{2+}, Ga^{3+}, Mg^{2+}, Ta^{5+}, and Al^{3+})[28−31] and nonmetallic (Br^-, Cl^-, and F^-)[32−34] ions to increase lattice electrical conductivity through partial reduction of Ti^{4+} to Ti^{3+}.

Received: November 30, 2020
Accepted: January 5, 2021
Published: January 14, 2021

https://dx.doi.org/10.1021/acsaem.0c02994
ACS Appl. Energy Mater. 2021, 4, 1894−1905

Several efforts have been investigated to increase the electrical conductivity of LTO through surface modifications via conductive coatings.[35−38] Although carbon-coatings offer a very efficient way to improve LTO anode rate capabilities, they also decrease cell's volumetric energy densities.[12,39] Furthermore, fabrication of uniform and optimized carbon coated LTO using economically facile techniques remains challenging.[12]

Syntheses of nano LTO particles including nanorods, nanotubes, and nanowires offers an efficient strategy to improve LTO electrochemical performance.[40−42] It is well-known that nanostructured active materials can enhance both electron and Li^+ migration by shortening diffusion pathways and providing excess surface lithium storage ascribed to their large surface areas and small sizes.[2,27] In addition, LTO NPs will have larger contact area between the electrolyte and electrode, resulting in improved intercalation kinetics. These phenomena contribute to enhance the rate capabilities of nanostructured LTO compared to bulk LTO. Multiple synthesis methods have been explored in efforts to prepare spinel LTO including sol−gel, hydrothermal synthesis, solution-combustion, and spray pyrolysis.[43−46] However, these routes often offer low yields, involve complicated procedures, high costs, and toxic precursors detracting from commercialization practicality.

Therefore, the synthesis of nanoscale LTO materials with controlled morphologies, phase purity, and using low-cost methods is highly desirable for assembly of LTO batteries. This provides the motivation to prepare LTO NPs using liquid-feed flame spray pyrolysis (LF-FSP).

Recent publications indicate that the introduction of appropriate amounts of solid electrolytes [$LiAlO_2$, $Li_{1.3}Al_{0.3}Ti_{1.7}(PO_4)_3$ (LATP), and $Li_{0.33}La_{0.56}TiO_3$] in to LTO anode is an effective, low-cost route to improve the electronic and ionic transport of LTO.[24,39,47] Thus, Han et al.[24] reported that added LATP can coat and/or bridge LTO particles, thereby facilitating Li^+ diffusion from electrolyte to the active material and improving electron migration to the current collector (Cu) by virtue of LATP's high ionic (6.2×10^{-5} S/cm)[48] and electronic conductivities (5×10^{-11} S/cm).[49] However, these studies use solid-state reaction methods (calcining >700 °C) to synthesize LTO-solid electrolyte composites, which makes it difficult to obtain nanostructured LTO particles as a result of particle necking.

Recently, we demonstrated that LF-FSP derived $LiAlO_2$ ceramic electrolytes offer optimal ionic conductivities (~10^{-6} S/cm) and electronic conductivities of 6.7×10^{-10} S/cm at ambient, both 3 orders of magnitude higher than those reported for LTO (Table 1).[50] Hence, LTO-$LiAlO_2$ composite anodes were prepared via simple ball-milling. We coincidentally reported the synthesis and characterization of a novel polymer electrolyte (Li_6SiON) derived from rice hull ash (RHA), an agricultural waste, providing a green route to all-solid-state batteries (Scheme 1).[51] In our effort to synthesize the Li_6SiON polymer electrolyte, we realized that it might also be possible to use this precursor to coat LTO NPs. The Li_6SiON electrolyte offers a room temperature (Table 1) ionic conductivity of 10^{-6} S/cm and electrical conductivity of 10^{-7} S/cm 6 orders of magnitude greater than that of LTO.

In this work, we synthesized high surface area (~38 m^2/g) spinel LTO NPs using LF-FSP. Contrary to the typical solid-state reaction, this method eliminates glass forming, grinding, and ball milling steps. In addition, LF-FSP derived LTO NPs are agglomerated but not necked which is crucial for facile dispersion and tape-casting. To enhance the electrical conductivity of LTO anodes, the LTO was mixed with flame made $LiAlO_2$ NPs (APS = 64 nm; 5 and 10 wt %) and coated with Li_6SiON polymer precursors (5 and 10 wt %).

To the best of our knowledge, this is the first time three component composite anodes, e.g., LTO-5$LiAlO_2$-10Li_6SiON, have been explored as an approach to improving LTO's rate capabilities. The composite anode exhibited a specific capacity of ~217 mAh/g at 5C for 500 cycles. The modified LTO NPs were characterized via XRD, XPS, SEM, EIS, and performance tests, as described in the following sections.

Table 1. Ionic and Electronic Conductivities of LTO, $LiAlO_2$, and Li_6SiON at Ambient

compounds	ionic conductivity (S/cm)	electronic conductivity (S/cm)	ref
LTO	10^{-13}−10^{-9}	$<10^{-13}$	22,23
$LiAlO_2$	10^{-6}	10^{-10}	50
Li_6SiON	10^{-6}	10^{-7}	51

2. EXPERIMENTAL SECTION

2.1. Synthesis of LTO NPs. The chemical products and analytical methods can be found in the Supporting Information.

The synthesis procedures for titanatrane{$Ti(OCH_2CH_2)_3N$-$[OCH_2CH_2N(CH_2CH_2OH)_2]$} and lithium propionate [$LiO_2CCH_2CH_3$] are discussed in our previous work.[52]

Lithium propionate (26.5 g) and titanatrane (236.8 g) were dissolved in anhydrous ethanol (1650 mL) to give a 3 wt % ceramic yield solution. To avoid the loss of lithium during the combustion process, excess lithium propionate (100 wt %) was used. The LF-FSP method was used to produce LTO NPs. A detailed description of LF-FSP process can be found elsewhere.[53]

The as-produced LTO NPs (10 g) were dispersed in anhydrous ethanol (350 mL) with 2 wt % poly(acrylic acid) using an ultrasonic horn (Vibra-cell VC 505 Sonics & Mater. Inc.) for 10−15 min operating at 100 W. The suspension was left to settle for 5 h to remove impurities and allow larger particles to settle. To remove the impurities the suspension was left to settle for 5 h and the recovered supernatant was dried at 100 °C/24 and heated to 700 °C/2 h/O_2, hereafter referred to as pristine LTO.

2.2. Preparation of LTO/$LiAlO_2$/Li_6SiON Composites. $LiAlO_2$ NPs were also synthesized using the LF-FSP method as discussed in our previous work.[50] We recently reported the direct distillative extraction of silica from RHA as the spirosiloxane, [SP = $(C_6H_6O_2)_2Si$]. SP reacts with $xLiNH_2$ to provide in oligomeric mixtures denoted as Li_xSiON (x = 2, 4, and 6) polymers with varying Li and N contents per Scheme 1. The Li_6SiON oligomers are for the most part soluble and stable in THF which makes it easier to coat LTO NPs, offering a simple and cost-effective green synthesis route to fabricate composite electrodes.

In our effort to enhance the electrical conductivity of LTO, composite anodes were processed by adding selected wt % $LiAlO_2$ solid and Li_6SiON polymer electrolytes during electrode formulation per Table 2.

The LTO and $LiAlO_2$ NPs (5 and 10 wt %) were dry ground for ~30 min in air to ensure uniform mixing. The LTO-$LiAlO_2$ mixtures, dispersed in anhydrous ethanol (5 mL), were ball-milled for 24 h using ZrO_2 beads (6 g, 3 mm) in 20 mL vial under nitrogen. The slurries were then heated at 100 °C/24 h/vacuum. In a separate step, LTO NPs and Li_6SiON polymer precursor (5 and 10 wt %) dissolved in THF then ultrasonicated at 100 W for 5−10 min. The recovered mixtures were then dried at 100 °C/24 h/vacuum. To evaluate the synergistic effects of the $LiAlO_2$ and Li_6SiON electrolytes, composite electrodes are synthesized by mixing the LTO-$LiAlO_2$ powders with

https://dx.doi.org/10.1021/acsaem.0c02994
ACS Appl. Energy Mater. 2021, 4, 1894−1905

Scheme 1. Synthesis of Li_xSiON Polymer Electrolyte

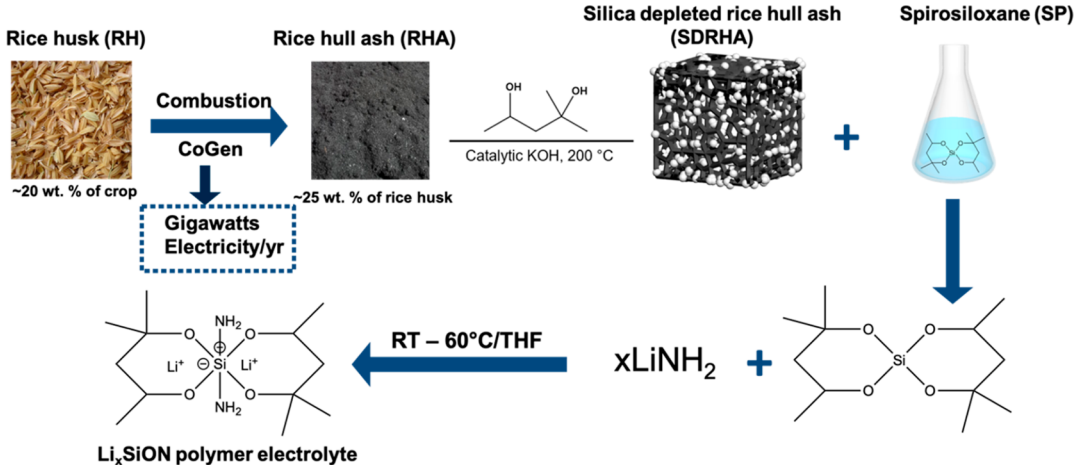

Table 2. Lists of Pristine and Composite Electrodes (wt %)

electrodes	$LiAlO_2$ (wt %)	Li_6SiON (wt %)
LTO	0	0
LTO-5$LiAlO_2$	5	0
LTO-10$LiAlO_2$	10	0
LTO-5Li_6SiON	0	5
LTO-10Li_6SiON	0	10
LTO-5$LiAlO_2$-5Li_6SiON	5	5
LTO-5$LiAlO_2$-10Li_6SiON	5	10
LTO-10$LiAlO_2$-5Li_6SiON	10	5
LTO-10$LiAlO_2$-10Li_6SiON	10	10

LTO-Li_6SiON powders. Scheme 2 depicts the preparation of the LTO-composite anode systems.

Scheme 2. Preparation of LTO-Composite Anodes

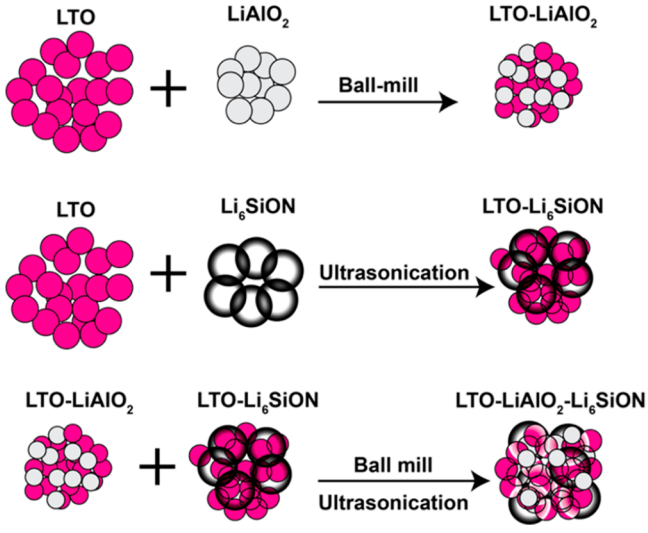

Before electrode fabrication, pristine LTO and carbon black (C-65) were heated to 100 °C/24 h/vacuum to remove trace moisture and eliminate oxygenated carbon species. Electrode slurries were prepared by mixing pristine LTO or LTO composites (80 wt %), C65 (10 wt %), and polyvinylidene fluoride [PVDF, (10 wt %)] in 1-methyl pyrrolidin-2-one.

The LTO-Li_6SiON mixtures were ultrasonicated for 10−15 min/N_2 to give homogeneous slurries. The LTO-$LiAlO_2$ mixtures were ball milled for 24 h using ZrO_2 beads (6 g) in 20 mL vials and then coated onto current collector (Cu foils, 16 μm). After drying at 80 °C/12 h/vacuum, the electrodes were cut into 8 mm discs, and thermo-pressed at 40−50 MPa/50 °C/5 min using a heated benchtop press (Carver, Inc.) to improve packing density. The electrodes have areal loading densities ranging from 3 to 4 mg/cm^2. LTO-composite-Li half cells were assembled following the standard coin cell procedure discussed elsewhere.[54]

3. RESULTS AND DISCUSSION

In this section, we primarily characterize pristine LTO NPs and composite anodes by XRD, FTIR, SEM, and TGA. In the second part, we discuss the electrochemical properties of half-cells assembled using the LTO-composite electrodes. The effect of the $LiAlO_2$ solid electrolyte and Li_6SiON polymer electrolyte additives on the rate performance of the LTO were also investigated.

3.1. Structure and Morphology of LTO Composites.

Figure S1 shows the XRD powder pattern of as-produced LTO NP composed primarily of spinel LTO phase (92 wt %). The weak diffraction peaks ~27.6° and 55.5° 2θ can be assigned to TiO_2 (rutile) and the small peak~ 20.3° 2θ is attributed to Li_2TiO_3.[55] The Figure S1 broad peaks at low 2θ angles decrease and the intensity of the peak corresponding to Li_2TiO_3 decreases on heating to 700 °C, suggesting formation of phase pure spinel LTO without impurities.

The XRD powder patterns of LTO-pristine, LTO-$LiAlO_2$, and LTO-Li_6SiON composites are shown in Figure 1. All the peaks can be indexed to the Fd3-m space group with a cubic lattice.[47] XRD of LTO-10$LiAlO_2$ (Figure 1a) powder exhibits broad and low-intensity peak ~21° and the doublet peaks at ~34° 2θ, which can be indexed to γ-$LiAlO_2$ (PDF: 04-009-6438). Conversely, no noticeable lattice fringes ascribed to the presence of $LiAlO_2$ are found due to its low content and the fact that the LTO-$LiAlO_2$ composite powder was produced through a simple ball-milling without any heat treatment.

Figure 1b shows the XRD plot of the Li_6SiON powder heated to 100 °C/12 h/vacuum. The broad peak centered at ~35° 2θ suggests the absence of crystalline structure.[51] Amorphous Li_6SiON generates no discernible diffraction peaks in the LTO-Li_6SiON composite powder. Figure S2 presents the XRD patterns of LTO-$LiAlO_2$−Li_6SiON composite powders. The lattice parameters for the LTO-$LiAlO_2$−Li_6SiON (a = 8.362 Å) powder are essentially the same as those of the pristine material (8.364 Å).

https://dx.doi.org/10.1021/acsaem.0c02994
ACS Appl. Energy Mater. 2021, 4, 1894−1905

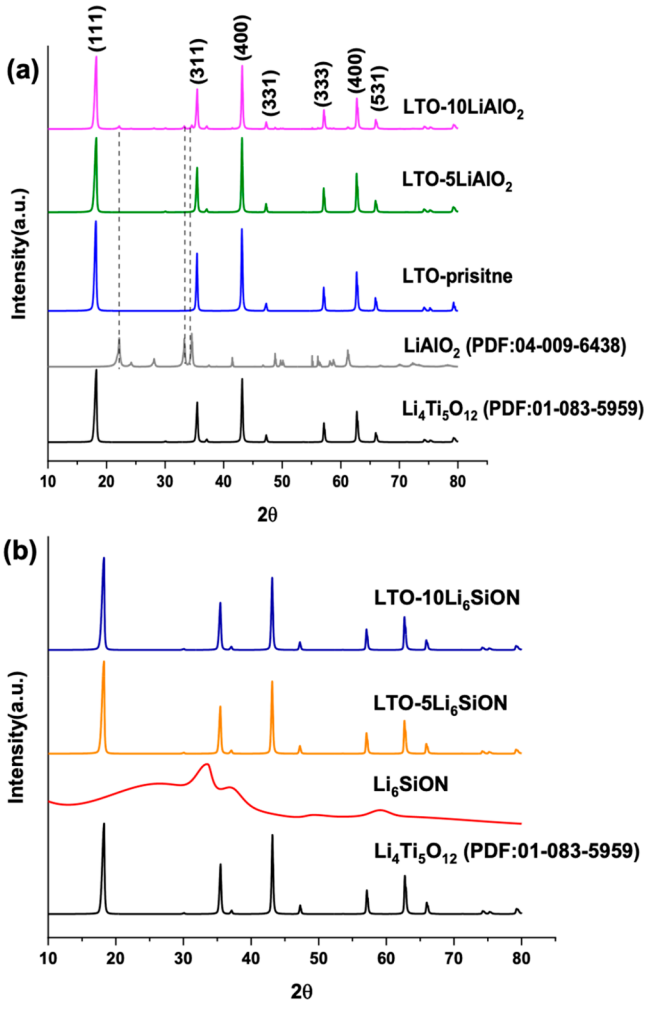

Figure 1. XRD plots of (a) LTO-pristine and LTO-$LiAlO_2$ and (b) LTO-Li_6SiON powders.

The FTIR spectra of LTO-pristine and LTO-composite powders are presented in Figure S3. The spectra of all samples change slightly with addition of $LiAlO_2$ and Li_6SiON polymer electrolytes. The broad peak ~1450−1500 cm^{-1} corresponds to carbonate $\nu C{=}O$, typical for LF-FSP derived powders.[50] The two broad absorption bands centered at 650 and 465 cm^{-1}, respectively, are due to the symmetric and asymmetric stretching vibrations of lattice $[MO_6]$ octahedral groups confirming the presence of spinel LTO.[56]

High performance LTO anodes are available using nanostructured materials because such materials offer larger contact areas with electrolyte, shorter diffusion distances for Li^+ and electrons, and excess near-surface lithium storage in comparison with micron-size LTO anodes.[27,41] The solid-state reaction method is simple; however, product quality is not satisfactory due to particle inhomogeneities, large APSs, and irregular morphologies. In contrast, we are able to the design and prepare uniform, nanoscale LTO electrodes for high performance applications.

Figure 2 shows SEMs of pristine LTO, LTO-composite powders. Powder morphologies of the pristine LTO (Figure 2a) and LTO-$LiAlO_2$ (Figure 2b,c) are similar agglomerates with uniform APSs < 60 nm. Table S1 lists the SSAs and APSs of the LTO-composite powders.

As noted above, high surface area is an important characteristic of nanostructured materials. The BET SSA of pristine LTO is 37 ± 0.8 m^2/g. The calculated APS using the BET surface area is ~46 nm for the pristine LTO. The LTO-10$LiAlO_2$ sample shows a slight decrease to 31 m^2/g and increase in APS (54 nm) attributed to the relatively larger $LiAlO_2$ APS (64 nm).[50]

Figure 2d,e shows highly dispersed small particles on the LTO particles, which indicates that the polymer electrolyte is coated on the LTO particles, supporting the EDX studies presented below. The powder surface morphology of the LTO-10$LiAlO_2$-10Li_6SiON composite reveals denser particle accumulation attributed to the polymer electrolyte additives.

The thermal stability of the composite powders was investigated by TGA. Figure S4 shows representative TGA plots (700 °C/10 °C min^{-1}/N_2) for pristine LTO and LTO-composite powders. The mass losses <250 °C are attributed to physi/chemisorbed water on the surfaces of the LTO-$LiAlO_2$ composite powders. The LTO-Li_6SiON composite powder exhibits relatively larger mass loss (8 wt %) from 100 to 450 °C ascribed to evaporation/or decomposition of organics. Figure S4c demonstrates that the TGA ceramic yield for the

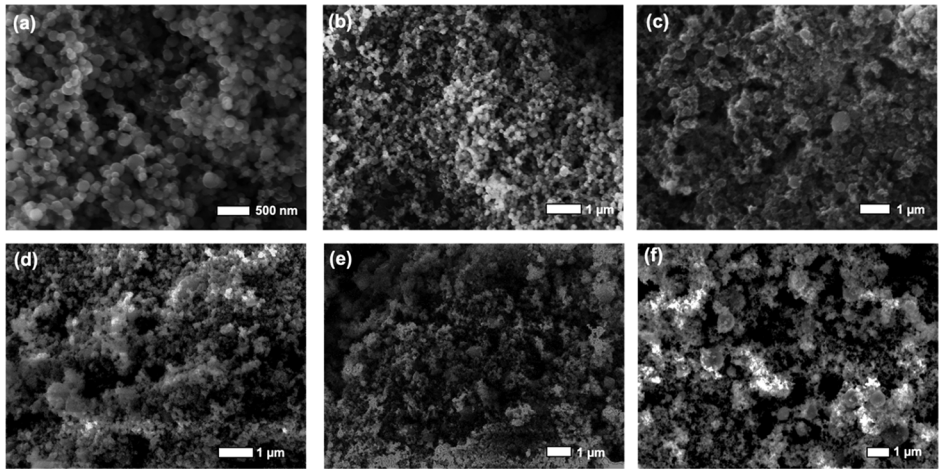

Figure 2. SEM images of pristine LTO (a), LTO-5$LiAlO_2$ (b), LTO-10$LiAlO_2$ (c), LTO-5Li_6SiON (d), LTO-10Li_6SiON (e), and LTO-10$LiAlO_2$-10Li_6SiON (f) powders.

https://dx.doi.org/10.1021/acsaem.0c02994
ACS Appl. Energy Mater. 2021, 4, 1894−1905

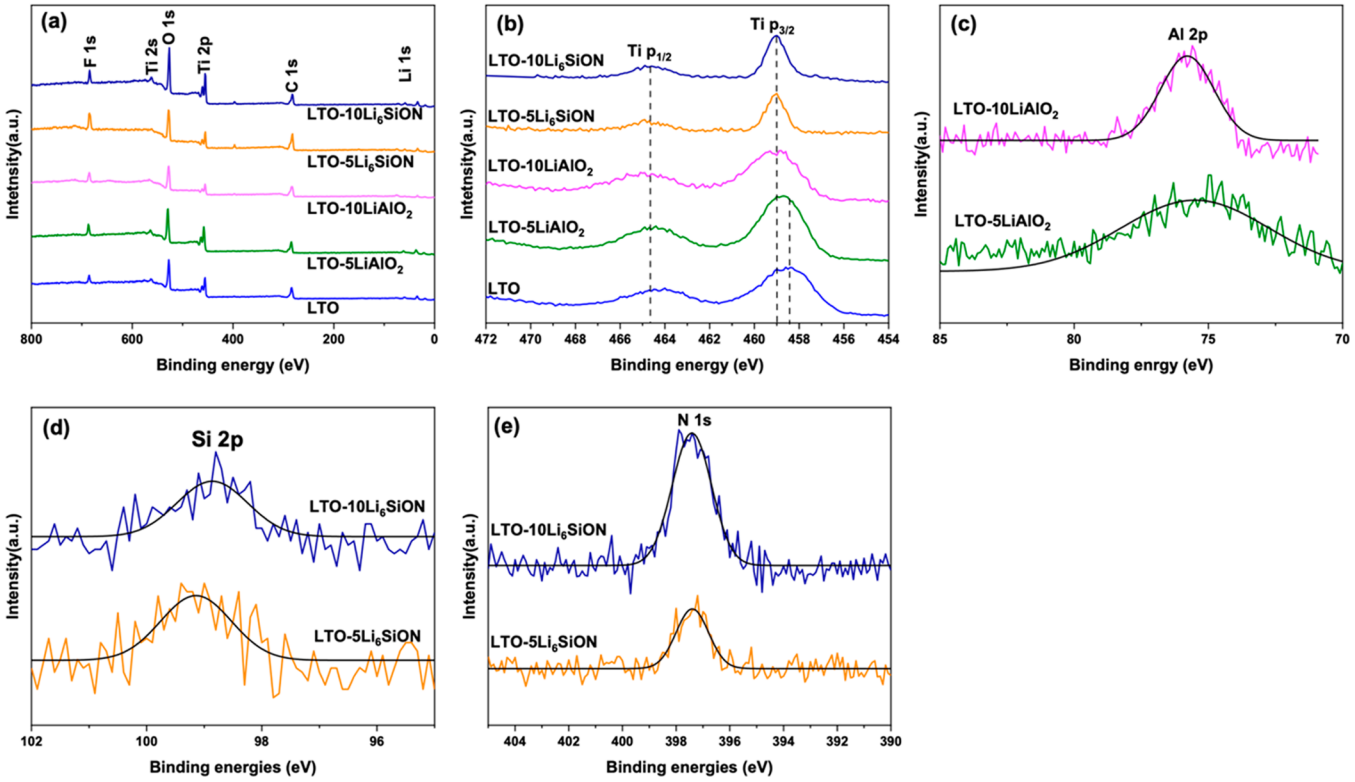

Figure 3. XPS survey spectra (a) and high resolution spectra of Ti 2p (b), Al 2p (c), Si 2p (d), and N 1s (e) for LTO, LTO-$LiAlO_2$, and LTO-Li_6SiON electrodes.

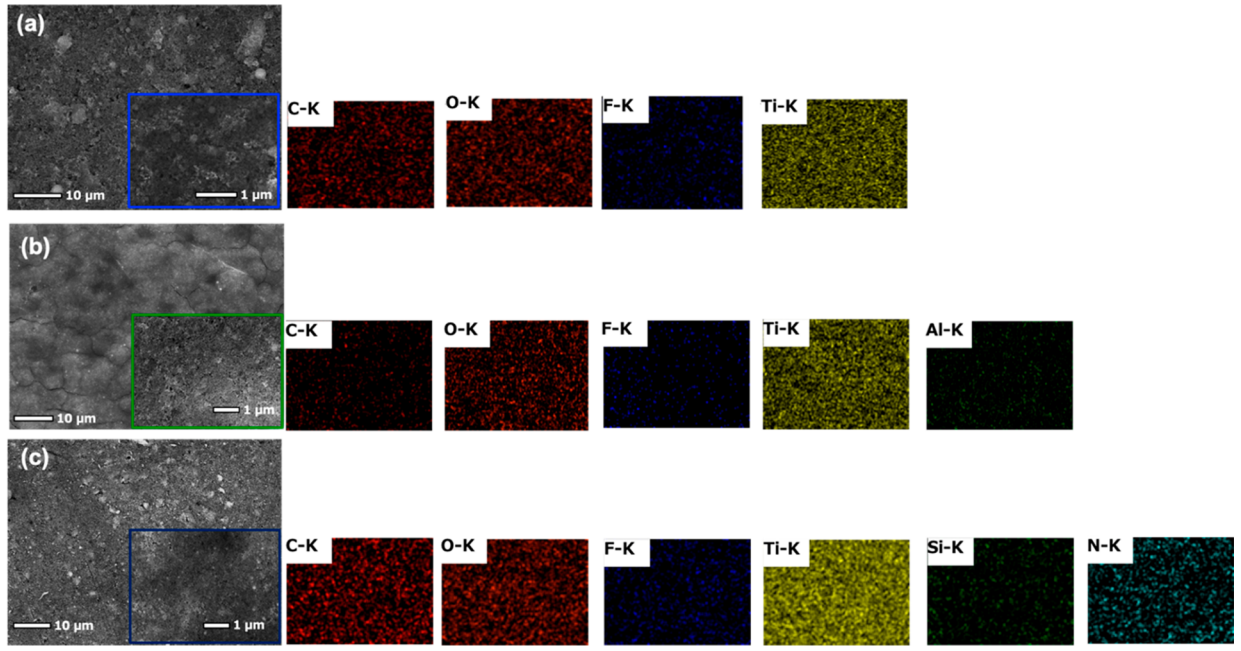

Figure 4. SEM and EDX images for the pristine LTO (a), LTO-5$LiAlO_2$ (b), and LTO-10Li_6SiON (c) electrodes.

LTO-composite powders are in good agreement with the theoretical ceramic yields calculated using the rule of mixtures.

3.2. Surface Characterization. The surface chemical composition and binding energies of the LTO-pristine and LTO-composite electrodes were analyzed by XPS. The survey spectra (Figure 3a) reveal signature elements (Li, Ti, C, and O) for the LTO-pristine and LTO-composite electrodes. All electrodes show a small F 1s peak (2.3−3.5 at. %) ascribed to the presence of PVDF. The resulting deduced elements from XPS are listed in Tables S2 and S3.

Figure 3b presents core resolution XPS spectra for electrode Ti 2p. Deconvoluted peaks at ∼464.4 and 458.5 eV corresponds to the Ti $2P_{1/2}$ and Ti $2P_{3/2}$ core level binding energies of Ti^{4+} of spinel LTO, respectively.[24,27] No noticeable change is observed in the Ti 2p core peak for the LTO-pristine and LTO-$LiAlO_2$ electrodes. The Ti $2p_{3/2}$ peak seems to shift

https://dx.doi.org/10.1021/acsaem.0c02994
ACS Appl. Energy Mater. 2021, 4, 1894−1905

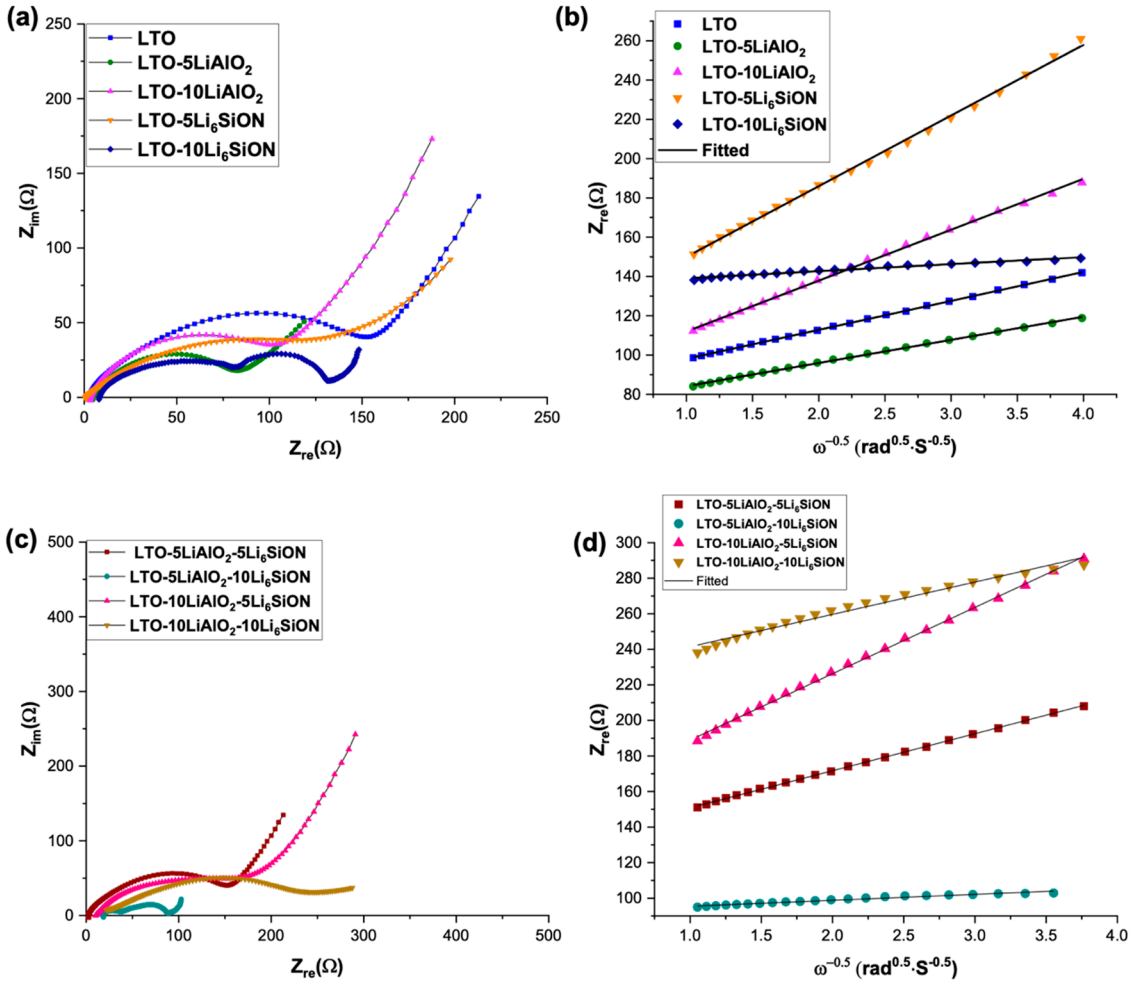

Figure 5. Nyquist plot of LTO composite−Li half-cell (a and c) and plot of Z_{re} vs angular frequency (b and d). The dotted line corresponds to the experimental value and the solid line indicates the fitted data.

slightly to higher binding energy (459 eV) for the LTO-Li_6SiON electrode compared to the pristine LTO electrode. This suggests that introducing the polymer electrolyte changes bonding at the LTO surface. Figure S5 deconvolutes the Ti 2p peak for the LTO-pristine and LTO-composite electrodes. The Ti^{3+} contents at $2p_{1/2}$ increase to 10.2 and 15.7% for the LTO-5Li_6SiON and LTO-10Li_6SiON electrodes, respectively, which are significantly higher than the content in LTO-pristine electrode. (4.2 wt %). This implies that Ti^{4+} is partially reduced to Ti^{3+} during the coating process. As noted above, the presence of Ti^{3+} in LTO can effectively improve electron−hole concentrations enhancing bulk electrical conductivity.[12,29] As a consequence, the LTO-Li_6SiON electrode exhibits superior electrical conductivity as discussed below.

The core level spectra of the Al 2p (74.8 eV) peak increases with increasing $LiAlO_2$ content (10 wt %), a consequence of $LiAlO_2$ particles associated with the surface of LTO particles (Figure 3c). The core level spectra of Si 2p (99 eV) are similar in shape and peak position for the LTO electrode coated with 5 and 10 wt % Li_6SiON polymer electrolytes as shown in Figure 3d. The overall atomic concentration of N (Figure 3e) increases with the introduction of 10 wt % Li_6SiON, suggesting that the LTO surface is coated uniformly with the polymer electrolyte.

The survey spectra (Figure S6) reveal signature peaks (Li, Ti, C, and O) for the LTO-$LiAlO_2$- Li_6SiON electrodes, while Al, Si, and N peaks are detected in the LTO composite electrodes ascribed to the presence of $LiAlO_2$ and Li_6SiON powders. The XPS derived compositions are listed in Table S4.

Figure 4a shows SEMs and EDX mapping of the pristine LTO electrode revealing a relatively porous microstructure. The EDX map presents uniform distribution of signature elements (C, O, F, and Ti), supporting the Figure 3a XPS studies. The elemental map of F results from the binder PVDF.

Figure 4b shows SEMs and EDX mapping of an LTO-5$LiAlO_2$ electrode revealing a relatively dense microstructure. The LTO-5$LiAlO_2$ electrode seems to offer a smoother morphology compared to the electrode with higher $LiAlO_2$ content. Careful examination of the 10 wt % $LiAlO_2$ modified electrode reveals some uneven $LiAlO_2$ coatings (Figure S7a). This might be ascribed to incomplete dispersion of the active particles with higher $LiAlO_2$ content. The EDX map presents uniform distribution of signature elements (C, O, Ti, F, and Al). The Al elemental map is also uniform for LTO-5$LiAlO_2$ in congruent with the XPS data (Figure 3c). Table S5 lists the deduced atomic percentages based on EDX analyses for the LTO electrodes. As expected, the Al at. % increased with increasing $LiAlO_2$ content.

https://dx.doi.org/10.1021/acsaem.0c02994
ACS Appl. Energy Mater. 2021, 4, 1894−1905

Figures 4c and S7b show SEM and EDX images of LTO + 5 and 10 wt % Li_6SiON electrodes, respectively. The Si and N elemental maps indicate uniform distributions for both electrodes corresponding with the XPS data (Figure 3d,e). As expected, the Si and N at. % increase with increased Li_6SiON content. The LTO-Li_6SiON electrodes show a relatively denser microstructure. Several notable experiments have demonstrated that the rate capability depends on the composition of additives, binder types, and degree of electrode compaction.[57] Besides being an additive with superior ionic and electronic conductivities, the Li_6SiON polymer electrolyte can behave like a binder promoting intimate contact between the LTO particles and the current collector. These properties strongly enhance the LTO rate performance as discussed below.

3.3. Electrochemical Characterization. Electrochemical impedance spectroscopy (EIS) was performed on the LTO composite electrode-Li half-cells before cycling. The corresponding Nyquist plots are presented in Figure 5a,c. The impedance curves were fitted using a modified Randle-Ershler equivalent circuit model (Figure S8). The Z' axis intercept of the Nyquist plot at high frequency region is attributed to the ohmic resistance (R_s), which corresponds to internal resistance of electrode and electrolyte. The charge transfer resistance (R_{ct}) is associated with the semicircle in the intermediate frequency region. The sloped line in the low frequency-region represent the Warburg impedance (W), corresponding to the solid-state diffusion resistance. The constant phase elements (CPE) are attributed to the double-layer capacitance. The diffusion coefficient (D_{Li}) of the LTO-composite electrodes were calculated using eqs S1−S3.[39]

All of the Nyquist spectra (Figures 5a,c) exhibit semicircles and tail in the high and low frequency regions, respectively. The electrical/ionic conductivity at the interface is represented by the R_{ct}, and the diffusion of Li^+ into the bulk of the active material is related to W. Appropriate $LiAlO_2$ (5 wt %) and Li_6SiON (10 wt %) modification improves the conduction of LTO anode as demonstrated in Figure 5. This suggests that surface modification enhances LTO conductivity and decreases R_{ct}. The EIS studies indicate that the LTO-5$LiAlO_2$ electrode have better Li^+ diffusion coefficient than than pristine LTO. However, the introduction of higher content $LiAlO_2$ (10 wt %) resulted in an increase in the R_{ct} and a decrease in Li^+ diffusion coefficient, which could be attributed to a thicker barrier that impeded the Li^+ migration at the LTO surface. It could also be ascribed to the increase in the APS of LTO-10$LiAlO_2$ (54 nm). The Li^+ diffusivity result can be compared (Table S6) to reported LTO-$LiAlO_2$ and LTO−$Li_{0.33}La_{0.56}TiO_3$ composite electrodes.[39,47]

The calculated Li^+ diffusion coefficients for pristine LTO, LTO-$LiAlO_2$, and LTO-Li_6SiON are listed in Table 3. LTO-5$LiAlO_2$-10Li_6SiON has the highest diffusion coefficient (~2.7×10^{-12}) among the LTO electrodes reported here. This study demonstrates that introduction of an appropriate amount of solid electrolyte enhances the electrochemical performance of LTO.

Figure 6a presents CV curves measured between 0 and 2.5 V (vs Li/Li^+) at a scan rate of 1 mV/s. Two typical cathodic/anodic peaks are observed ~1.8/1.5 V for all samples, corresponding to the two-phase LTO redox reaction mechanism of LTO ($Li_4Ti_5O_{12} + 3Li^+ + 3e^- \rightleftarrows Li_7Ti_5O_{12}$). This suggests that the introduction of $LiAlO_2$ and Li_6SiON polymer electrolyte does not change LTO electrochemistry

Table 3. List of Diffusivities and Potential Gap for Pristine and Composite LTO Electrodes

electrodes	$D_{Li}(cm^2/s)$	$\Delta\varphi_p$ (mV)
LTO-pristine	$4.6 \pm 0.5 \times 10^{-14}$	400
LTO-5$LiAlO_2$	$6.1 \pm 0.7 \times 10^{-13}$	340
LTO-10$LiAlO_2$	$4.8 \pm 0.2 \times 10^{-14}$	410
LTO-5Li_6SiON	$6.7 \pm 0.6 \times 10^{-14}$	380
LTO-10Li_6SiON	$1.2 \pm 0.3 \times 10^{-12}$	320
LTO-5$LiAlO_2$ - 5Li_6SiON	$2.3 \pm 0.3 \times 10^{-13}$	300
LTO-5$LiAlO_2$ −10Li_6SiON	$2.7 \pm 0.3 \times 10^{-12}$	290
LTO-10$LiAlO_2$ - 5Li_6SiON	$3.0 \pm 0.5 \times 10^{-14}$	350
LTO-10$LiAlO_2$ - 10Li_6SiON	$1.3 \pm 0.6 \times 10^{-14}$	370

(Figure 6b). Two additional weak redox peaks in the range of 0.4−0.6 V are ascribed to the multistep restoration of Ti^{4+}.[58] This is attributed to the insertion of additional Li^+ ions to the $Li_7Ti_5O_{12}$ (rock-salt) to transform to $Li_{8.5}Ti_5O_{12}$ (quasi-rock-salt) reducing all $Ti^{4+}$to Ti^{3+}.[59]

Table 3 also lists the peak parameters for the composite electrodes in the CV plots. The degree of polarization is reflected by the voltage difference between anodic and cathodic peaks. LTO-5$LiAlO_2$-10Li_6SiON exhibits the smallest potential gap ($\Delta\varphi_p$ = 0.29 V) between reduction and oxidation peaks compared tos the pristine LTO electrode (($\Delta\varphi_p$ = 0.4 V). This suggests that the composite electrode has lower electrochemical polarization and better diffusion kinetics than LTO-pristine. This is ascribed to faster Li^+ and electron transfer processes imparted by the ceramic and polymer electrolyte additives. This is consistent with the excellent rate capability of the LTO-5$LiAlO_2$-10Li_6SiON composite electrode.

The electrochemical performance of LTO-pristine, LTO-$LiAlO_2$, LTO-Li_6SiON, and LTO-$LiAlO_2$−Li_6SiON electrodes was investigated by galvanostatic cycling test at different C-rates (0.5, 1, and 5 C) between 1 and 2.5 V. Pristine LTO (Figure 7a) shows an initial discharge capacity of ~180 mAh/g at 0.5 C. The reversible capacity at 0.5 C rate is ~154 mAh/g after 100 cycles, which is 88% of the theoretical capacity. This is in good agreement with previous reports and corresponds to the transformation of $Li_4Ti_5O_{12}$ to $Li_7Ti_5O_{12}$.[12]

The discharge capacity for pristine LTO half-cell decreases to ~125 mAh/g at 5 C. However, capacities for LTO-5$LiAlO_2$ and LTO-10Li_6SiON fade slowly remaining stable at 146 and 160 mAh/g at 5C, respectively. The LTO-5$LiAlO_2$-10Li_6SiON exhibits a discharge capacity (~140 mAh/g) at 5 C. On the whole, the LTO-Li_6SiON and LTO-$LiAlO_2$ electrodes reveal enhanced rate capacity relative to pristine LTO.

After 100 cycles, the specific capacities are 155 ± 0.7, 142 ± 1.4, 156 ± 0.5, and 162 ± 0.2 mAh/g at 0.5 C for the half-cells assembled with LTO-5$LiAlO_2$, LTO-10$LiAlO_2$, LTO-5Li_6SiON, and LTO-10Li_6SiON electrodes, respectively. The reversible capacities of LTO-Li_6SiON decrease slowly compared to those for LTO-$LiAlO_2$ and the pristine LTO electrodes. However, the LTO-10$LiAlO_2$-5Li_6SiON and LTO-10$LiAlO_2$-10Li_6SiON composite electrodes show relatively low discharge capacities of 127 and 131 mAh/g after 100 cycles.

To understand the reason why the LTO−10$LiAlO_2$-5Li_6SiON and LTO−10$LiAlO_2$-10Li_6SiON capacities (Figure 7b) decrease after 70 cycles, the discharge/charge curves for the selected cycles were investigated (Figure S9). The polarization degree of the composite electrode was explored by calculating the voltage difference (ΔE) between discharge

https://dx.doi.org/10.1021/acsaem.0c02994
ACS Appl. Energy Mater. 2021, 4, 1894−1905

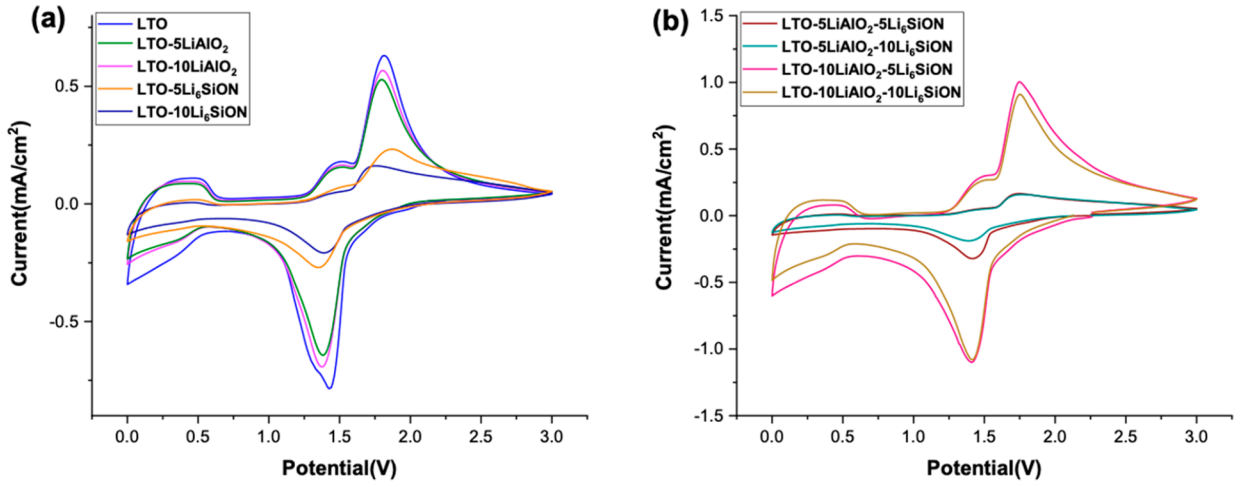

Figure 6. Cyclic voltammograms of the LTO-pristine, LTO-$LiAlO_2$, and LTO-Li_6SiON (a) and LTO-$LiAlO_2$−Li_6SiON (b) half-cells.

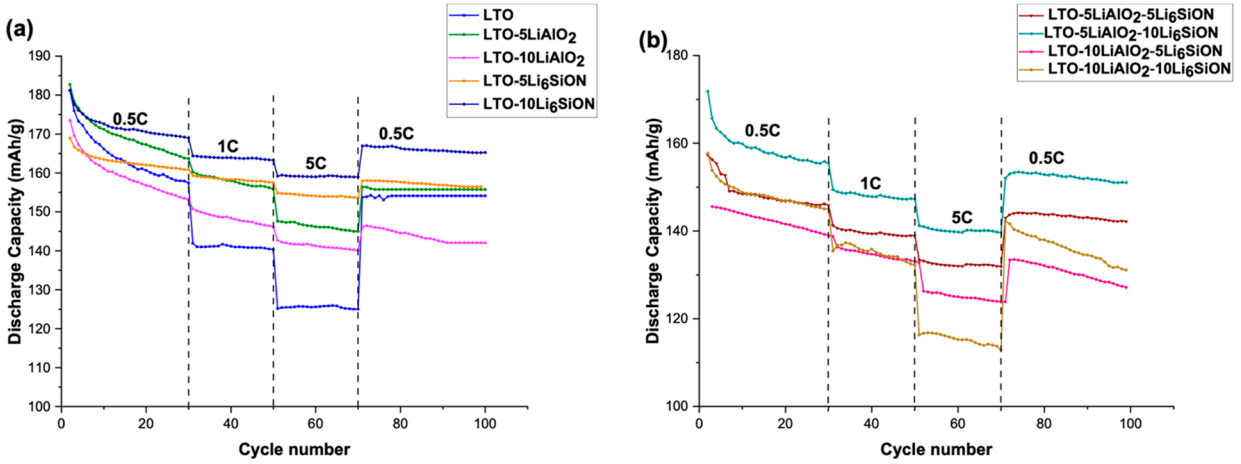

Figure 7. Cycling performance of the LTO-pristine, LTO-$LiAlO_2$, and LTO-Li_6SiON (a) and LTO-$LiAlO_2$−Li_6SiON (b) half-cells cycled between 1 and 2.5 V.

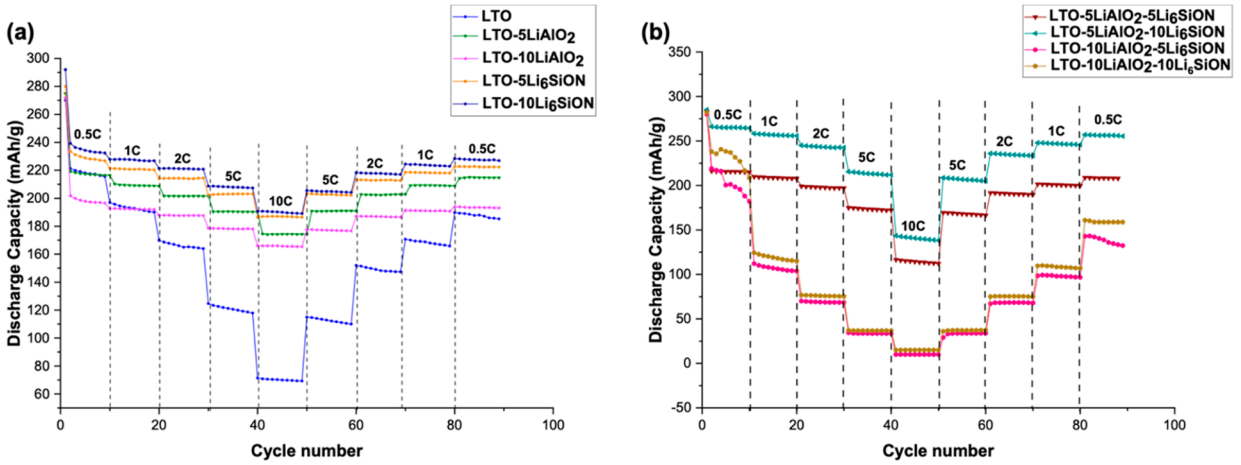

Figure 8. Cycling performance of the, LTO-$LiAlO_2$, and LTO-Li_6SiON (a) and LTO-$LiAlO_2$−Li_6SiON (b) half-cells cycled between 0.01 and 2.5 V.

and charge plateaus. As presented in Figures S9 and S10, the ΔE of LTO−10$LiAlO_2$-10Li_6SiON increases gradually with increasing cycle number ($\Delta E \approx 70$ mV), indicating relatively higher degrees of polarization compared to the LTO−5$LiAlO_2$-10Li_6SiON electrode ($\Delta E \approx 50$ mV) after 70 cycles. This might be ascribed to the larger quantity $LiAlO_2$, which significantly reduces the amount of active material LTO, resulting in lower capacity retention. This is consistent with what is reported in the literature for LTO-$LiAlO_2$ (10 wt %) composite electrodes.[47] In addition, as discussed above in the

https://dx.doi.org/10.1021/acsaem.0c02994
ACS Appl. Energy Mater. 2021, 4, 1894−1905

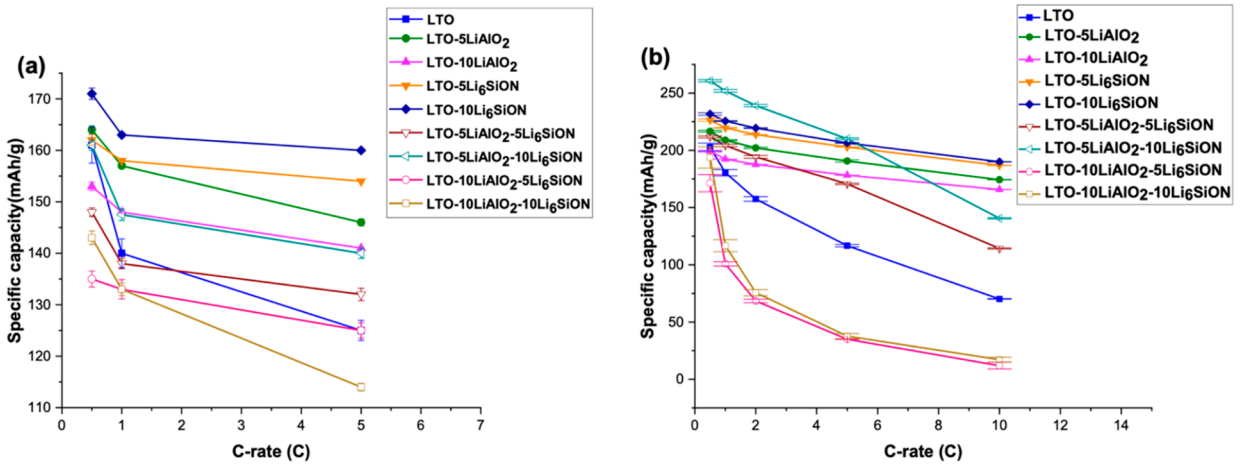

Figure 9. Comparison of discharge capacities of the various electrodes cycled between 1.0 and 2.5 V (a) and 0.01 and 2.5 V (b) at selected C-rates.

diffusivity section, the LTO-10$LiAlO_2$-10Li_6SiON composite did not show a high Li^+ diffusivity coefficient when compared to the LTO-5$LiAlO_2$-10Li_6SiON electrode.

Figure 8 presents the rate performance of the LTO-pristine and LTO-composite electrodes cycled in the range of 0.01−2.5 V. The initial discharge capacity of all of the half-cells is greater than the theoretical capacity (260 mAh/g). This extra capacity may be attributed to the formation of a solid electrolyte interface (SEI), intercalation of Li^+ into the conductive carbon black (C65), and decomposition of the organic liquid electrolyte. The LTO electrodes (Figure 8a) display excellent cycling stability for both cutoff voltages (0.01 and 1 V), suggesting that the lithiation of the rock-salt structure is highly reversible.

The reversible capacities found for LTO-5$LiAlO_2$-10Li_6SiON (260 mAh/g) and LTO-10Li_6SiON (231 mAh/g) are much higher than those of LTO-pristine electrodes (202 mAh/g) at 0.5 C as demonstrated in Figure 8b. LTO-5$LiAlO_2$-10Li_6SiON maintains a high discharge capacity of 255 mAh/g at 0.5C, which is much higher than the pristine LTO (185 mAh/g) after 90 cycles. At 10 C, the LTO-10Li_6SiON shows the highest discharge capacity of 190 mAh/g. The LTO-5$LiAlO_2$ also delivered a high specific capacity of 174 mAh/g, which is more than double the capacity obtained for the pristine LTO (70 mAh/g). The introduction of appropriate amounts of $LiAlO_2$ NPs shortens diffusion distances for Li^+ and electrons, increases the contact interface with electrolyte, and provides abundant surface Li^+ storage sites or excess near-surface Li^+ storage.

Figure 9 demonstrates the rate capability of LTO-pristine and LTO composite electrodes cycled with different voltage windows at various current densities. The LTO-pristine half-cell cycled between 1.0 and 2.5 V potential range (Figure 9a) delivered average specific capacity of 160 mAh/g at 0.5 C. The pristine LTO half-cell was also discharged to 0.01 V delivering reversible capacities of 202 and 120 mAh/g at 0.5 and 5 C as shown in Figure 9b, respectively. These electrochemical results indicate that LF-FSP derived LTO powders enable high rate performance at different discharge voltage ranges.

Figure 9a,b shows that the LTO-10$LiAlO_2$-5Li_6SiON and LTO-10$LiAlO_2$-10Li_6SiON composite electrodes show poor discharge capacities compared to the pristine LTO electrode when discharged to different voltages. This suggests that $LiAlO_2$ enhances the rate performance of the LTO-composite electrodes. Hence, it is important that the optimal content of $LiAlO_2$ (5 wt %) is introduced to achieve superior cell performance. Compared to pristine LTO, $Li_4Ti_5O_{12}$−$LiAlO_2$ (5 wt %),[47] and $Li_4Ti_5O_{12}$−$Li_{0.33}La_{0.56}TiO_3$ (5 wt %)[39] composites prepared by solid-state reactions, the rate capability of LF-FSP derived LTO-5$LiAlO_2$-10Li_6SiON composite electrodes is much higher in the range of 0.01−2.5 V at higher C-rates (Table 4). This clearly indicates that moderate modification of LTO particle surfaces is substantially beneficial to rate performance.

Table 4. Comparison of Discharge Capacities of LTO-Composite Anode Materials at 5 C

electrodes	discharge capacities (mAh/g)	ref
LTO-$LiAlO_2$ (5 wt %)	127	47
LTO-$LiAlO_2$ (10 wt %)	∼50	47
LTO-$Li_{0.33}La_{0.56}TiO_3$ (5 wt %)	146	39
LTO-$Li_{0.33}La_{0.56}TiO_3$ (10 wt %)	137	39
$Li_4Ti_{4.9}La_{0.1}O_{12}$	181	61
LTO-TiO_2	117	62
LTO-TiO_2/C	140	63
LTO-5$LiAlO_2$	190	this work
LTO-10Li_6SiON	206	this work
LTO-5$LiAlO_2$-10Li_6SiON	217	this work

Figure S11 show the Nyquist plots of the half-cells in delithiation state after 100 cycles. Table S7 lists the electrolyte resistance (R_e) and R_{ct} of these half-cells. The R_{ct} values of LTO-5$LiAlO_2$-10Li_6SiON decreases markedly, suggesting the enhanced Li^+ diffusion due to the introduction of electrolytes with optimal electrical conductivity than pristine LTO anode. Zhang et al.[60] suggest that local charge imbalance promotes the electron transfer; hence, the modification of LTO surface enhances the electronic conductivity.

The high rate performance of the LTO-5$LiAlO_2$-10Li_6SiON electrodes is attributed to

1. Optimal amounts of $LiAlO_2$ (5 wt %) and Li_6SiON (10 wt %) between or on the LTO particle surfaces enhancing the ionic conductivity as demonstrated by the increase in lithium ion diffusivity. (Table 3).

https://dx.doi.org/10.1021/acsaem.0c02994
ACS Appl. Energy Mater. 2021, 4, 1894−1905

2. Li_6SiON polymer electrolyte reorganizing LTO surface bonding, resulting in an increase in the electronic conductivity due to the local change imbalance.
3. Diminishing electrode polarization, via introduction of appropriate $LiAlO_2$ and Li_6SiON electrolyte contents.
4. *The enhanced electrical conductivities of electrolyte additives coupled with uniform particle morphology and high surface area of LTO NPs resulted in long-term cycling stability over 500 cycles delivering reversible capacity of ∼217 mAh/g at 5 C (Figure S12).*

4. CONCLUSIONS

Herein, a facile LF-FSP method enabled the synthesis of high surface area, phase pure LTO NPs using a low-cost precursor. Pristine LTO was mixed with $LiAlO_2$ and Li_6SiON electrolytes to improve the ionic and electronic conductivity by simple ball-milling and ultrasonication methods. The microstructure studies show that the composite powders are homogeneous with particle sizes <60 nm. XPS and EDX studies further confirm that the surface of the LTO particles is uniformly coated with the polymer electrolyte. By virtue of the high electrical conductivity of $LiAlO_2$ and Li_6SiON electrolyte, the LTO composite electrodes with optimal $LiAlO_2$ (5 wt %) and Li_6SiON (10 wt %) electrolyte additives exhibit excellent rate performance delivering reversible capacity of 260 and 140 mAh/g at 0.5 and 10 C, respectively.

■ ASSOCIATED CONTENT

Supporting Information

The Supporting Information is available free of charge at https://pubs.acs.org/doi/10.1021/acsaem.0c02994.

Supplemental XRD, FTIR, XPS, TGA, and SEM data (PDF)

■ AUTHOR INFORMATION

Corresponding Author

Richard M. Laine − *Department of Materials Science and Engineering, University of Michigan, Ann Arbor, Michigan 48109-2136, United States;* orcid.org/0000-0003-4939-3514; Phone: +1 734 764 6203; Email: talsdad@umich.edu; Fax: +1 734 763 4788

Authors

Eleni Temeche − *Department of Materials Science and Engineering, University of Michigan, Ann Arbor, Michigan 48109-2136, United States*

Elizaveta Buch − *Group Research, Daimler AG (Mercedes-Benz Cars), 71034 Boeblingen, Germany*

Xinyu Zhang − *Department of Materials Science and Engineering, University of Michigan, Ann Arbor, Michigan 48109-2136, United States*

Taylor Brandt − *Department of Materials Science and Engineering, University of Michigan, Ann Arbor, Michigan 48109-2136, United States*

Andreas Hintennach − *Group Research, Daimler AG (Mercedes-Benz Cars), 71034 Boeblingen, Germany*

Complete contact information is available at: https://pubs.acs.org/10.1021/acsaem.0c02994

Author Contributions

The manuscript was written with contributions from all authors.

Author Contributions

Dedicated to the memory of Professor Dr. Dr. Andreas Hintennach, deceased May 10, 2020, a mentor and friend.

Notes

The authors declare no competing financial interest.

■ ACKNOWLEDGMENTS

We are grateful for the support of a significant portion of this work by a gift from Mercedes-Benz Research & Development North America (MBRDNA). A portion of this work was also supported by a DMR NSF Grant No. DMR project 1926199. We also like to thank the University of Michigan Rackham Merit Fellowship (RMF) program. We also acknowledge the financial support of the University of Michigan College of Engineering and NSF Grant No. DMR-0402785 (XPS) and technical support from the Michigan Center for Materials Characterization. We especially thank Dr. Greg Less for helping us with coin cell cycling. We also would like to thank Wadham Energy LP for providing the RHA powders. We also like to thank Dylan Edelman for processing and collecting NPs.

■ REFERENCES

(1) Zubi, G.; Dufo-López, R.; Carvalho, M.; Pasaoglu, G. The Lithium-Ion Battery: State of the Art and Future Perspectives. *Renewable Sustainable Energy Rev.* **2018**, *89*, 292.

(2) Nitta, N.; Wu, F.; Lee, J. T.; Yushin, G. Li-Ion Battery Materials: Present and Future. *Mater. Today* **2015**, *18*, 252.

(3) Tarascon, J. M.; Armand, M. Issues and Challenges Facing Rechargeable Lithium Batteries. *Materials for Sustainable Energy: A Collection of Peer-Reviewed Research and Review Articles from Nature Publishing Group* **2010**, 171.

(4) Ma, L.; Hendrickson, K. E.; Wei, S.; Archer, L. A. Nanomaterials: Science and Applications in the Lithium-Sulfur Battery. *Nano Today* **2015**, *10*, 315.

(5) Uhlmann, C.; Illig, J.; Ender, M.; Schuster, R.; Ivers-Tiffée, E. In Situ Detection of Lithium Metal Plating on Graphite in Experimental Cells. *J. Power Sources* **2015**, *279*, 428.

(6) Liu, Q.; Du, C.; Shen, B.; Zuo, P.; Cheng, X.; Ma, Y.; Yin, G.; Gao, Y. Understanding Undesirable Anode Lithium Plating Issues in Lithium-Ion Batteries. *RSC Adv.* **2016**, *6*, 88683.

(7) Aurbach, D.; Zinigrad, E.; Cohen, Y.; Teller, H. A Short Review of Failure Mechanisms of Lithium Metal and Lithiated Graphite Anodes in Liquid Electrolyte Solutions. *Solid State Ionics* **2002**, *148*, 405.

(8) Doughty, D.; Roth, E. P. A General Discussion of Li Ion Battery Safety *Electrochem. Soc. Interface* **2012**. DOI: 10.1149/2.F03122if.

(9) Aravindan, V.; Lee, Y.-S.; Madhavi, S. Research Progress on Negative Electrodes for Practical Li-Ion Batteries: Beyond Carbonaceous Anodes. *Adv. Energy Mater.* **2015**, *5*, 1402225.

(10) Pfanzelt, M.; Kubiak, P.; Fleischhammer, M.; Wohlfahrt-Mehrens, M. TiO2 Rutile - An Alternative Anode Material for Safe Lithium-Ion Batteries. *J. Power Sources* **2011**, *196*, 6815.

(11) Zuo, X.; Zhu, J.; Müller-Buschbaum, P.; Cheng, Y. J. Silicon Based Lithium-Ion Battery Anodes: A Chronicle Perspective Review. *Nano Energy* **2017**, *31*, 113.

(12) Sun, X.; Radovanovic, P. V.; Cui, B. Advances in Spinel Li4Ti5O12 Anode Materials for Lithium-Ion Batteries. *New J. Chem.* **2015**, *39*, 38.

(13) Yi, T. F.; Jiang, L. J.; Shu, J.; Yue, C. B.; Zhu, R. S.; Qiao, H. Bin. Recent Development and Application of Li4Ti5O 12 as Anode Material of Lithium Ion Battery. *J. Phys. Chem. Solids* **2010**, *71*, 1236.

(14) Zhao, B.; Ran, R.; Liu, M.; Shao, Z. A Comprehensive Review of Li4Ti5O12-Based Electrodes for Lithium-Ion Batteries: The Latest Advancements and Future Perspectives. *Mater. Sci. Eng., R* **2015**, *98*, 1.

(15) Zhang, Q.; Li, X. Recent Developments in the Doped-Li4Ti5O12 Anode Materials of Lithium-Ion Batteries for Improving the Rate Capability *Int. J. Electrochem. Sci.* **2013**.
(16) Zaghib, K.; Simoneau, M.; Armand, M.; Gauthier, M. Electrochemical Study of Li4Ti5O12 as Negative Electrode for Li-Ion Polymer Rechargeable Batteries. *J. Power Sources* **1999**, *81-82*, 300.
(17) Mukai, K.; Kato, Y.; Nakano, H. Understanding the Zero-Strain Lithium Insertion Scheme of Li[Li 1/3Ti5/3]O4: Structural Changes at Atomic Scale Clarified by Raman Spectroscopy. *J. Phys. Chem. C* **2014**, *118*, 2992.
(18) Sandhya, C. P.; John, B.; Gouri, C. Lithium Titanate as Anode Material for Lithium-Ion Cells: A Review. *Ionics* **2014**, *20*, 601.
(19) Yuan, T.; Tan, Z.; Ma, C.; Yang, J.; Ma, Z. F.; Zheng, S. Challenges of Spinel Li4Ti5O12 for Lithium-Ion Battery Industrial Applications. *Adv. Energy Mater.* **2017**, *7*, 1601625.
(20) Yao, X. L.; Xie, S.; Chen, C. H.; Wang, Q. S.; Sun, J. H.; Li, Y. L.; Lu, S. X. Comparisons of Graphite and Spinel Li1.33Ti1.67O 4 as Anode Materials for Rechargeable Lithium-Ion Batteries. *Electrochim. Acta* **2005**, *50*, 4076.
(21) Xiang, H. F.; Jin, Q. Y.; Wang, R.; Chen, C. H.; Ge, X. W. Nonflammable Electrolyte for 3-V Lithium-Ion Battery with Spinel Materials LiNi0.5Mn1.5O4 and Li4Ti5O12. *J. Power Sources* **2008**, *179*, 351.
(22) Chen, C.; Vaughey, J.; Jansen, A.; Dees, D.; Kahaian, A.; Goacher, T.; Thackeray, M. Studies of Mg-Substituted Li42xMgx-Ti5O12 Spinel Electrodes (0 × 1) for Lithium Batteries. *J. Electrochem. Soc.* **2001**, *148*, A102.
(23) Zhao, L.; Hu, Y. S.; Li, H.; Wang, Z.; Chen, L. Porous Li4Ti5O12 Coated with N-Doped Carbon from Ionic Liquids for Li-Ion Batteries. *Adv. Mater.* **2011**, *23*, 1385.
(24) Han, J. P.; Zhang, B.; Wang, L. Y.; Zhu, H. L.; Qi, Y. X.; Yin, L. W.; Li, H.; Lun, N.; Bai, Y. J. Li1.3Al0.3Ti1.7(PO4)3 Behaving as a Fast Ionic Conductor and Bridge to Boost the Electrochemical Performance of Li4Ti5O12. *ACS Sustainable Chem. Eng.* **2018**, *6* (6), 7273−7282.
(25) Gao, J.; Jiang, C.; Ying, J.; Wan, C. Preparation and Characterization of High-Density Spherical Li4Ti5O12 Anode Material for Lithium Secondary Batteries. *J. Power Sources* **2006**, *155*, 364.
(26) Bai, X.; Li, W.; Wei, A.; Li, X.; Zhang, L.; Liu, Z. Preparation and Electrochemical Properties of Mg2+ and F− Co-Doped Li4Ti5O12 Anode Material for Use in the Lithium-Ion Batteries. *Electrochim. Acta* **2016**, *222*, 1045.
(27) Tian, Q.; Zhang, Z.; Yang, L.; Xiang, Y. Improving the Lithium Storage Properties of Li4Ti5O12anodes by Facile Two-Phase Formation and Nanostructure Engineering Strategy. *J. Alloys Compd.* **2017**, *705*, 638−644.
(28) Wolfenstine, J.; Allen, J. L. Electrical Conductivity and Charge Compensation in Ta Doped Li4Ti5O12. *J. Power Sources* **2008**, *180*, 582.
(29) Ji, S.; Zhang, J.; Wang, W.; Huang, Y.; Feng, Z.; Zhang, Z.; Tang, Z. Preparation and Effects of Mg-Doping on the Electrochemical Properties of Spinel Li4Ti5O12 as Anode Material for Lithium Ion Battery. *Mater. Chem. Phys.* **2010**, *123*, 510.
(30) Zhao, H.; Li, Y.; Zhu, Z.; Lin, J.; Tian, Z.; Wang, R. Structural and Electrochemical Characteristics of Li4-XAlxTi5O12 as Anode Material for Lithium-Ion Batteries. *Electrochim. Acta* **2008**, *53*, 7079.
(31) Lee, B.; Yoon, J. R. Preparation and Characteristics of Li4Ti5O 12with Various Dopants as Anode Electrode for Hybrid Supercapacitor. *Curr. Appl. Phys.* **2013**, *13*, 1350.
(32) Huang, S.; Wen, Z.; Gu, Z.; Zhu, X. Preparation and Cycling Performance of Al3+and F- Co-Substituted Compounds Li4AlxTi5-XF YO12-Y. *Electrochim. Acta* **2005**, *50*, 4057.
(33) Salvatore, K. L.; Lutz, D. M.; Guo, H.; Yue, S.; Gan, J.; Tong, X.; Liu, P.; Takeuchi, E. S.; Takeuchi, K. J.; Marschilok, A. C.; Wong, S. S. Solution-Based, Anion-Doping of Li4Ti5O12 Nanoflowers for Lithium-Ion Battery Applications. *Chem. - Eur. J.* **2020**, *26*, 9389.
(34) Qi, Y.; Huang, Y.; Jia, D.; Bao, S. J.; Guo, Z. P. Preparation and Characterization of Novel Spinel Li4Ti5O12-XBrx Anode Materials. *Electrochim. Acta* **2009**, *54*, 4772.
(35) Li, X.; Qu, M.; Huai, Y.; Yu, Z. Preparation and Electrochemical Performance of Li4Ti5O12/Carbon/Carbon Nano-Tubes for Lithium Ion Battery. *Electrochim. Acta* **2010**, *55*, 2978.
(36) Wang, G. J.; Gao, J.; Fu, L. J.; Zhao, N. H.; Wu, Y. P.; Takamura, T. Preparation and Characteristic of Carbon-Coated Li4Ti5O12 Anode Material. *J. Power Sources* **2007**, *174*, 1109.
(37) Jung, H. G.; Kim, J.; Scrosati, B.; Sun, Y. K. Micron-Sized, Carbon-Coated Li4Ti5O12 as High Power Anode Material for Advanced Lithium Batteries. *J. Power Sources* **2011**, *196*, 7763.
(38) Luo, H.; Shen, L.; Rui, K.; Li, H.; Zhang, X. Carbon Coated Li4Ti5O12 Nanorods as Superior Anode Material for High Rate Lithium Ion Batteries. *J. Alloys Compd.* **2013**, *572*, 37.
(39) Zhu, Y. R.; Yuan, J.; Zhu, M.; Hao, G.; Yi, T. F.; Xie, Y. Improved Electrochemical Properties of Li4Ti5O12-Li0.33La0.56-TiO3 Composite Anodes Prepared by a Solid-State Synthesis. *J. Alloys Compd.* **2015**, *646*, 612−619.
(40) Poizot, P.; Laruelle, S.; Grugeon, S.; Dupont, L.; Tarascon, J. M. Nano-Sized Transition-Metal Oxides as Negative-Electrode Materials for Lithium-Ion Batteries. *Nature* **2000**, *407*, 496.
(41) Wang, Y.; Liu, H.; Wang, K.; Eiji, H.; Wang, Y.; Zhou, H. Synthesis and Electrochemical Performance of Nano-Sized Li 4Ti5O12 with Double Surface Modification of Ti(III) and Carbon. *J. Mater. Chem.* **2009**, *19*, 6789.
(42) Jaiswal, A.; Horne, C. R.; Chang, O.; Zhang, W.; Kong, W.; Wang, E.; Chern, T.; Doeff, M. M. Nanoscale LiFePO[Sub 4] and Li[Sub 4]Ti[Sub 5]O[Sub 12] for High Rate Li-Ion Batteries. *J. Electrochem. Soc.* **2009**, *156*, A1041.
(43) Shen, C. M.; Zhang, X. G.; Zhou, Y. K.; Li, H. L. Preparation and Characterization of Nanocrystalline Li4Ti5O12 by Sol-Gel Method. *Mater. Chem. Phys.* **2003**, *78*, 437.
(44) Zhou, Q.; Liu, L.; Tan, J.; Yan, Z.; Huang, Z.; Wang, X. Synthesis of Lithium Titanate Nanorods as Anode Materials for Lithium and Sodium Ion Batteries with Superior Electrochemical Performance. *J. Power Sources* **2015**, *283*, 243.
(45) Ju, S. H.; Kang, Y. C. Characteristics of Spherical-Shaped Li4Ti5O12 Anode Powders Prepared by Spray Pyrolysis. *J. Phys. Chem. Solids* **2009**, *70*, 40.
(46) Chou, S. L.; Wang, J. Z.; Liu, H. K.; Dou, S. X. Rapid Synthesis of Li4Ti5O12 Microspheres as Anode Materials and Its Binder Effect for Lithium-Ion Battery. *J. Phys. Chem. C* **2011**, *115*, 16220.
(47) Fang, Z. K.; Zhu, Y. R.; Yi, T. F.; Xie, Y. Li4Ti5O12-LiAlO2 Composite as High Performance Anode Material for Lithium-Ion Battery. *ACS Sustainable Chem. Eng.* **2016**, *4* (4), 1994−2003.
(48) Monchak, M.; Hupfer, T.; Senyshyn, A.; Boysen, H.; Chernyshov, D.; Hansen, T.; Schell, K. G.; Bucharsky, E. C.; Hoffmann, M. J.; Ehrenberg, H. Lithium Diffusion Pathway in Li1.3Al0.3Ti1.7(PO4)3 (LATP) Superionic Conductor. *Inorg. Chem.* **2016**, *55*, 2941.
(49) Wu, X. M.; Li, X. H.; Wang, S. W.; Wang, Z.; Zhang, Y. H.; Xu, M. F.; He, Z. Q. Preparation and Characterization of Lithium-Ion-Conductive Li1.3Al0.3Ti1.7(PO4)3 Thin Films by the Solution Deposition. *Thin Solid Films* **2003**, *425*, 103.
(50) Temeche, E.; Indris, S.; Laine, R. M. LiAlO2/LiAl5O8 Membranes Derived from Flame Synthesized Nanopowders as a Potential Electrolyte and Coating Materials for All Solid-State Batteries (ASSBs). *ACS Appl. Mater. Interfaces* **2020**, *12*, 46119.
(51) Zhang, X.; Temeche, E.; Laine, R. M. LixSiON (X= 2, 4, 6); A Novel Solid Electrolyte System Derived from Agricultural Waste. *Green Chem.* **2020**, *22*, 7491.
(52) Yi, E.; Wang, W.; Mohanty, S.; Kieffer, J.; Tamaki, R.; Laine, R. M. Materials That Can Replace Liquid Electrolytes in Li Batteries: Superionic Conductivities in Li1.7Al0.3Ti1.7Si 0.4P2.6O12. Processing Combustion Synthesized Nanopowders to Free Standing Thin Films. *J. Power Sources* **2014**, *269*, 577−588.
(53) Temeche, E.; Yi, E.; Keshishian, V.; Kieffer, J.; Laine, R. M. Liquid-Feed Flame Spray Pyrolysis Derived Nanopowders (NPs) as a

https://dx.doi.org/10.1021/acsaem.0c02994
ACS Appl. Energy Mater. 2021, 4, 1894−1905

Route to Electrically Conducting Calcium Aluminate (12CaO.7Al2O3) Films. *J. Eur. Ceram. Soc.* **2019**, *39*, 1263.
(54) Temeche, E.; Yu, M.; Laine, R. M. Silica Depleted Rice Hull Ash (SDRHA), an Agricultural Waste, as a High-Performance Hybrid Lithium-Ion Capacitor. *Green Chem.* **2020**, *22*, 4656.
(55) Alias, N. A.; Kufian, M. Z.; Teo, L. P.; Majid, S. R.; Arof, A. K. Synthesis and Characterization of Li4Ti5O12. *J. Alloys Compd.* **2009**, *486*, 645.
(56) Prosini, P. P.; Mancini, R.; Petrucci, L.; Contini, V.; Villano, P. Li4Ti5O12 as Anode in All-Solid-State, Plastic, Lithium-Ion Batteries for Low-Power Applications. *Solid State Ionics* **2001**, *144*, 185.
(57) Du, Z.; Wood, D. L.; Daniel, C.; Kalnaus, S.; Li, J. Understanding Limiting Factors in Thick Electrode Performance as Applied to High Energy Density Li-Ion Batteries. *J. Appl. Electrochem.* **2017**, *47*, 405.
(58) Yi, T. F.; Shu, J.; Zhu, Y. R.; Zhu, X. D.; Zhu, R. S.; Zhou, A. N. Advanced Electrochemical Performance of Li4Ti4.95V0.05O12 as a Reversible Anode Material down to 0 V. *J. Power Sources* **2010**, *195*, 285.
(59) Tian, B.; Xiang, H.; Zhang, L.; Wang, H. Effect of Nb-Doping on Electrochemical Stability of Li 4Ti 5O 12 Discharged to 0 V. *J. Solid State Electrochem.* **2012**, *16*, 205.
(60) Zhang, Q.; Verde, M. G.; Seo, J. K.; Li, X.; Meng, Y. S. Structural and Electrochemical Properties of Gd-Doped Li4Ti5O12 as Anode Material with Improved Rate Capability for Lithium-Ion Batteries. *J. Power Sources* **2015**, *280*, 355.
(61) Yi, T. F.; Xie, Y.; Wu, Q.; Liu, H.; Jiang, L.; Ye, M.; Zhu, R. High Rate Cycling Performance of Lanthanum-Modified Li 4Ti 5O 12 Anode Materials for Lithium-Ion Batteries. *J. Power Sources* **2012**, *214*, 220.
(62) Rahman, M. M.; Wang, J. Z.; Hassan, M. F.; Chou, S.; Wexler, D.; Liu, H. K. Basic Molten Salt Process-A New Route for Synthesis of Nanocrystalline Li4Ti5O12-TiO2 Anode Material for Li-Ion Batteries Using Eutectic Mixture of LiNO3-LiOH-Li2O2. *J. Power Sources* **2010**, *195*, 4297.
(63) Wang, J.; Zhao, H.; Yang, Q.; Wang, C.; Lv, P.; Xia, Q. Li4Ti5O12-TiO2 Composite Anode Material for Lithium-Ion Batteries. *J. Power Sources* **2013**, *222*, 196.

https://dx.doi.org/10.1021/acsaem.0c02994
ACS Appl. Energy Mater. 2021, 4, 1894−1905